Journal of Solid State Chemistry **145,** 186–196 (1999)
Article ID jssc.1999.8241, available online at http://www.idealibrary.com on IDEAL®

Bidimensional Cationic Ordering and Thermal Dependence in β-$Pb_xV_2O_5$ Bronzes

Olivier Mentré,[1] Marielle Huvé, and Francis Abraham

Laboratoire de Cristallochimie et Physicochimie du Solide, URA CNRS 452, ENSCL, Université des Sciences et Technologies de Lille, BP 108, 59652 Villeneuve d'Ascq Cedex, France

Received July 27, 1998; in revised form February 11, 1999; accepted February 26, 1999

The monoclinic lead vanadium oxide bronzes β-$Pb_xV_2O_5$ were investigated for their cationic ordering within the host lattice. Superstructure reflections appear on X-ray powder patterns beyond $x \approx 0.30$. For the formal $x = 0.30$ lead ratio, the crystal structure was refined from X-ray single crystal data in the (a, $2b$, c) unit cell, $a = 15.478(10)$ Å, $2b = 7.288(5)$ Å, $c = 10.123(6)$ Å, $\beta = 109.29(1)^\circ$, S. G. $P2_1/m$, and final $R = 0.047$, $R_w = 0.054$. It shows evidence of an intratunnel ordering involving a Pb^{2+} zigzag sequence running parallel to the b axis while ordered and disordered tunnels alternate along the a axis. Pb^{2+} display different interaction with the V–O framework according to the kind of tunnels it occupies. Electron diffraction patterns confirmed our X-ray results. A supplementary $2a$ periodicity was sometimes observed in small crystals as a subcondition of the previous ordering. Weissenberg photographs and electronic diffraction patterns allowed the proposition of a bidimensional cationic ordering model in the fourfold ($2a$, $2b$, c) unit cell. In that case, the intertunnel ordering involves strong local Pb^{2+} electrostatic effects despite the shielding of the tunnel walls. The thermal analysis (DTA and high temperature electronic microscopy) evidenced the irreversible disappearing of the superstructure on heating while a second rearrangement is observed on cooling.

INTRODUCTION

Vanadium oxide bronzes, namely $M_xV_2O_5$, were intensively studied for their physical properties (electric, thermoelectric, magnetic, etc.) (1–3) as well as for their structural liability. Effectively, the V–O framework can accommodate a wide variety of cations including $M = Li^+$, Na^+, K^+, Ca^{2+}, Cu^{2+}, Ag^+, Cd^{2+}, Pb^{2+} … and resulting in a large range of structural forms depending on the M nature, the x ratio, and the synthesis process (4). For instance, V_2O_5 is recognized to be particularly well suited for lithium insertions leading to the $Li_xV_2O_5$ system (5–9) that appeared promising as positive electrode material for secondary lithium batteries (10, 11). This system is especially complex and exhibits four forms (α-, β-, β'-, γ-) after a 650°C solid state reaction while α-, ε-, and δ-$Li_xV_2O_5$ are room-temperature prepared (12). As a matter of fact, the relationship of the number of structural types with the starting V_2O_5 is more or less obvious. They usually conserve the initial ≈ 3.6 Å lattice parameter representative of the distance between opposite vertices of the VO_6 octahedron. It is noticeable that in the V_2O_5 crystal structure, the oxygen polyhedra are better described as VO_5 square pyramids after excluding a long V–O distance, 2.79 Å (13). In any case, the 3.6 Å structural repeat may be doubled by ordering of interestial cations and vacancies. Such a phenomenon is suggested to occur during the two different ε-$Li_xV_2O_5$ varieties transition, $\varepsilon 1 \rightarrow \varepsilon 2$ (14). In this case, XRD experiments cannot reveal this kind of ordering because of the weak Li scattering factor. Thus Pb^{2+} is a good candidate for cationic ordering detection taking account of its scattering factor. Moreover, its large size and stereoctive lone pair effect act in favor of strong electrostatic repulsion driving superstructure formation. The $Pb_xV_2O_5$ system was first investigated by Darriet *et al.*, in 1969 (15). During their study only two single-phase domains were identified in solid state syntheses. α-$Pb_xV_2O_5$, with $0 < x \leq 0.01$, is orthorhombic while $0.15 \leq x \leq 0.33$ leads to the preparation of the monoclinic form β-$Pb_xV_2O_5$. The structure of the $x = 0.193$ term of the β-series was refined and confirmed the initial β-$Na_xV_2O_5$ structural model refined by Wadsley (16). Later, in 1990, Kato *et al.*, refined the crytal structure of $Pb_{0.33}V_2O_5$ in the same average unit cell (17). In contrast to the earlier studies (15, 16), Kato *et al.*, observed diffraction from a superstructure, with extra reflections $h/2k + 1/2l$. connected by diffuse scattering lines trending parallel to a^*. Probability calculations based on the intensity of diffuse lines using the formula of Kakinoki and Komura (18) let them propose a possible short-ordered Pb^{2+} arrangement.

In this paper, we present a refinement of the crystal structure of $Pb_{0.30}V_2O_5$, of which we have examined both polycrystalline samples and small single crystals. A high

[1] To whom correspondence should be addressed.

0022-4596/99 $30.00

degree of long-range order allows us to propose a commensurate superstructure with Pb^{2+}-vacancy ordering on (2*a*, 2*b*) supercell. Transmission electronic microscopy study was performed to confirm the XRD results. Finally the thermal dependence of the ordering was studied by high temperature electronic diffraction and DTA.

EXPERIMENTAL

Preparation and Equipment

The first evidences of superstructure in lead bronzes, originally giving inspiration to this study, were observed on products obtained from the new $Pb_2V_3O_9$ oxide (19) crystal growth attempts. A mixture of PbO, VO_2, and V_2O_5 in a 2:1:1 molar ratio was heated at 700°C over two days and cooled by switching off the furnace (preparation A). It gave rise to an inhomogeneous product including needle-shaped crystals identified as a monoclinic β-bronze-like compound.

Powder samples of $Pb_xV_2O_5$ ($x = 0.25, 0.30, 0.33$) were obtained from heating of stoichiometric mixtures of PbO, V_2O_5, and VO_2 in evacuate silica tubes according to the equation: $x\ \ PbO + (1-x)V_2O_5 + 2x\ \ VO_2 \rightarrow Pb_xV_2O_5$. The reaction was continued at 550°C for 3 days; then the furnace was cut off corresponding to an intermediate treatment between slow cooling and quenching. The X-ray diffraction powder patterns were obtained using a Siemens D5000 diffractometer (Cu$K\alpha$ radiation) equipped with a diffracted beam, graphite crystal back monochromator. The unit cell parameters were refined from data provided by the patterns.

In order to get single crystals possessing the greatest possible lead content we also prepared $Pb_{0.4}V_2O_5$ composition, despite the theoretical $x = 0.33$ maximal limit for the Pb β-bronze phases (15). This absolute maximum is explained in more details in the discussion section. The starting charge was then kept over 3 days at 750°C and slowly cooled to room temperature, 20°C/h (preparation B).

DTA was performed on a Setaram TG/TD 96-16.18 analysis system under a 2 l/h argon flow to prevent vanadium oxidation on heating.

Electron diffraction (ED) was performed on a JEOL 200CX electron microscope equipped with an eucentric goniometer ($+/-60°$).

Single Crystal X-Ray Analysis

A number of single crystals of preparation A were visually isolated and X-ray tested. The preliminary oscillation and Weissenberg studies indicated a systematic *b*-axis doubling compared to the reported β-bronze unit cell. However, additional *a*-axis doubling was observed in only one out of the single crystals. Unfortunately, the small dimensions of this crystal did not allow us to obtain sufficient information for a conventional X-ray diffraction data collection. Therefore, we used clues deduced from the Weissenberg photographs in the last section of this work dealing with the *a*-axis doubling. The largest single crystal $300 \times 23 \times 15\ \mu m^3$ was selected from the preparation B reaction product. After it was mounted on a glass fiber with the *b*-axis as the rotation axis, oscillation and Weissenberg photographs confirmed its ordered nature involving a primitive monoclinic unit cell ($a = 15.37$ Å, $b = 7.27$ Å, $c = 10.10$ Å, and $\beta = 109.3°$). Substructure reflections showed by systematic absences $h + k = 2n + 1$. It is in complete agreement with the $C2/m$ space group for β-bronze series. X-ray diffraction data were collected on a Nonius CAD-4 automatic diffractometer in half of the reciprocal space of the supercell under the conditions given in Table 1. The intensity of each reflection was corrected for Lorentz and polarization effects. The absorption corrections were performed using the analytical method of De Meulenaer and Tompa (20).

TABLE 1
Data, Intensity Measurement, and Structure Refinement Parameters for $Pb_{0.30}V_2O_5$

Crystal data	$Pb_{0.30}V_2O_5$	
Crystal symmetry	Monoclinic	
Space group	$P2_1/m$	
Cell dimension (Å)	$a = 15.478(10)$, $b = 7.288(5)$, $c = 10.123(6)$ $\beta = 109.29(1)°$	
Volume ($Å^3$)	1077.8	
Density (calc, $g.cm^{-3}$)	4.51	
Z	12	
Data collection		
Equipment	Nonius CAD-4	
1 (Mo$K\alpha$ (graphite monochromator)	0.7107 Å	
Scan mode	ω-2θ	
Scan width (°)	$1.30 + 0.34 \tan\theta$	
θ range (°)	2–35	
Standard reflections	600, $2\bar{4}\bar{2}$, $\bar{5}0\bar{1}$, $3\bar{2}0$, $3\bar{2}0$	
Measured every 2 hours (no decay)		
Recording reciprocal space	$-24 \le h \le 24$, $-11 \le k \le 11$, $0 \le 1 \le 16$	
Number of measured reflections	10029	
Number of reflections $I > 3\sigma(I)$	3827 (1695)	
Number of independent reflections	2196 (971)	
$\mu(cm^{-1})$ (for $\lambda K\alpha = 0.7107$ Å)	204	
Limiting faces and distances (mm)	010, $0\bar{1}0$	0.15
from arbitrary origin	100, $\bar{1}00$	0.0075
	001, $00\bar{1}$	0.0114
Transmissions factor range	0.19–0.75	
Merging R factor	0.039	
Refinement		
Number of refined parameters	100	
$R = \sum[\lvert Fo - Fc\rvert]/\sum\lvert Fo\rvert$	0.047	
$R_w = [\sum w(\lvert Fo\rvert - \lvert Fc\rvert)^2/\sum wFo^2]^{1/2}$	0.054	
With $w = 1/\sigma(Fo)$		

TABLE 2
Average Positional and Isotropic or Equivalent Thermal Parameters for $Pb_{0.30}V_2O_5$

Atom	Site and occupancy	x	y	z	B_{eq} (Å^2)
Pb	4(*i*), 0.451(2)	0.00433(4)	0	0.39454(6)	1.11(1)
V(1)	4(*i*), 1	0.33531(7)	0	0.0982(1)	0.45(2)
V(2)	—	0.11721(8)	0	0.1157(1)	0.67(2)
V(3)	—	0.28448(7)	0	0.4081(1)	0.49(2)
O(1)	2(*a*), 1	0	0	0	0.97(15)
O(2)	4(*i*), 1	0.8133(3)	0	0.0504(4)	0.68(9)
O(3)	—	0.6337(3)	0	0.0776(4)	0.52(9)
O(4)	—	0.4351(3)	0	0.2161(5)	1.10(10)
O(5)	—	0.2629(3)	0	0.2219(4)	0.58(8)
O(6)	—	0.1096(3)	0	0.2728(5)	1.08(10)
O(7)	—	0.7564(3)	0	0.4245(5)	0.83(10)
O(8)	—	0.3944(3)	0	0.4699(5)	1.27(11)

The structure refinement was first achieved in the subcell after sorting out hkl, $k = 2n + 1$ supercell reflections. Thus the 12 independent atoms of the $C2/m$ Wadsley (16) β-bronze crystallographic model were introduced in the refinement process. The occupancy of the Pb atom was refined to 0.451(2) leading to the formal $Pb_{0.30}V_2O_5$ stoichiometry. In the last cycles, the refinement of the secondary extinction and the introduction of anisotropic displacement parameters yielded the final $R = 0.030$ and $R_w = 0.038$. The atomic coordinates and equivalent isotropic thermal parameters are shown in Table 2. The atomic scattering factors for neutral atoms were taken from "International Tables for X-Ray Crystallography" (21) and the values for the anomalous dispersion corrections from Cromer and Liberman (22). The full-matrix least-squares refinement was performed with a local modification of the SFLS-5 program (23).

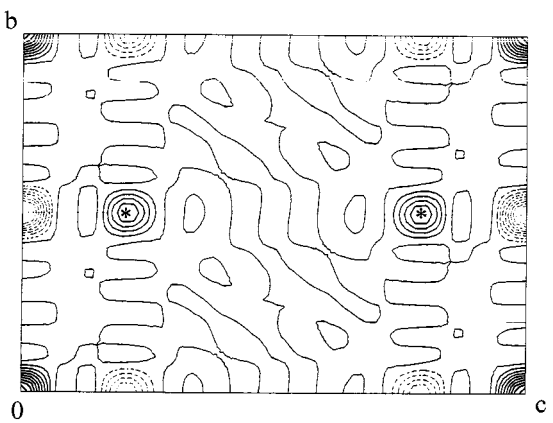

FIG. 1. Difference Patterson section calculated at $x = 0$ in arbitrary units; the broken lines indicate the observed minima.

b-Axis Doubling

According to the crystal structure, the b-doubling is related to the setting of a cationic ordering over two unit cells. The only systematic extinction disclosed for the whole bunch of collected reflections is $0k0$, $k = 2n$ involving possible $P2_1$ and $P2_1/m$ supercell space groups. The Pb^{2+} location was investigated by an extension of the difference Patterson function (DP), first reported by Frueh (24) to facilitate the solution of order–disorder problems. Effectively it was shown that under restriction applicable to our case, $P(u, v, w)_{\text{supercell}} - P(u, v, w)_{\text{subcell}} = P(u, v, w)_{\text{supercell-subcell}}$. Consequently, a Patterson synthesis was calculated using the 2132 superlattice-only reflections, k odd. This calculation provides rich results about likely and unlikely interatomic vectors. Considering the 4(*i*), ($\approx$ 0, 0, 0.39) Pb^{2+} location inside the $C2/m$ subcell, the b-doubling would yield seven possible Pb–Pb vectors (0, 0, 0.22), (0, 1/2, 0.22) (0, 1/2, 0), (1/2, 1/4, 0.22), (1/2, 3/4, 0.22), (1/2, 1/4, 0), and (1/2, 3/4, 0),

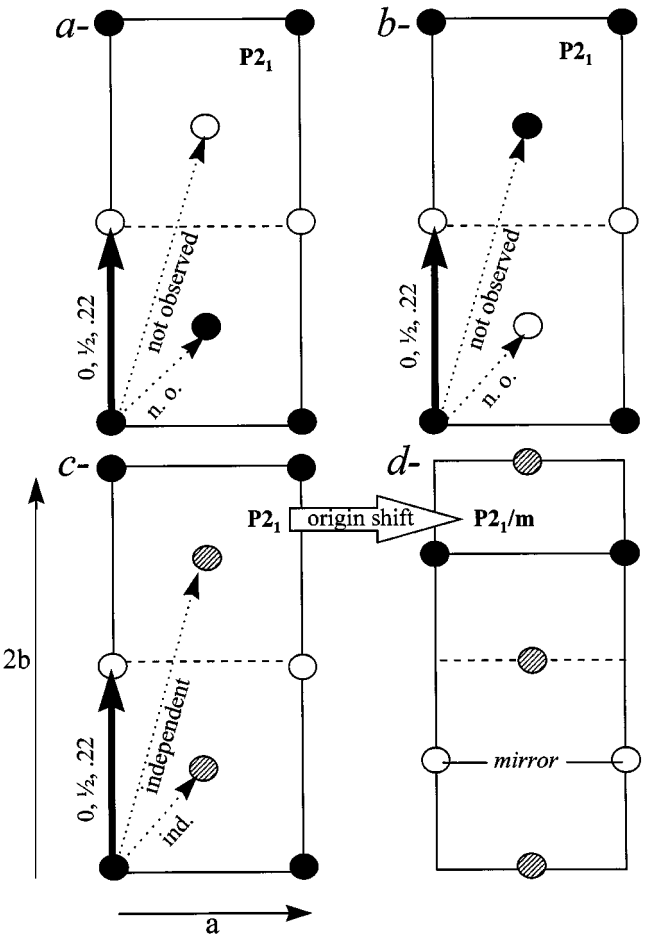

FIG. 2. (a, b) First tested and finally refuted Pb^{2+} distribution involving the $P2_1$ space group. (c) Partially disordered model ($P2_1$). (d) (0, 1/4, 0) origin shift leading to the conventional $P2_1/m$ space group. (●) $z = 0.39$, (○) $z = 0.61$, (▨) disordered over $z = 0.39$ and 0.61.

for $0 \leq w \leq 1/2$. Out of this list, the first vector is not relevant to the supercell. The intensities calculated on the DP map shown in Fig. 1 indicate a strong maximum at (0, 1/2, 0.22) and a minimum at (0, 1/2, 0) while the four latter possible vectors do not show any sign of electron density. Thus, different lead arrangement models were tested and confirmed the validity of our DP calculation. Pb^{2+} cations were located in different stages.

Model A: two independent lead atoms were introduced and refined as presented in Fig. 2a. This hypothesis, asserting the acentric $P2_1$ space group, did not converge, yielding $R = 0.17$ and $R_w = 0.22$. Actually such an arrangement would involve strong difference Patterson peaks at (1/2, 3/4, 0.22) and (1/2, 1/4, 0) that were not observed. It would therefore match good with the strong maximum and minimum of the DP maps. For symmetrical reasons, the refinement of the equivalent Model B presented in Fig. 2b also failed.

Model C: from the absence of any (1/2**a** + 1/4**b**) and (1/2**a** + 3/4**b**) composed interatomic vectors, we deduce complete crystallographic independence between $x = 0$ and $x = 1/2$ atoms that respectively correspond to hosts of a tunnel (see discussion section) and of the next one. Thus, Model C involving two independent Pb atoms in the $P2_1/m$ space group satisfies all the requested conditions (Fig. 2c). A shift of the origin to 0, 1/4, 0 (Fig. 2d) was therefore carried out to allow the use of a likely origin on the center of symmetry. Every 4(*i*) atom of the V–O subcell framework was split into three independent supercell positions using the relation: $C2/m$: 4(*i*) $(x, 0, z)_{sub} \rightarrow P2_1/m$: 4(*f*) $(1/2 + x, \approx 1/2, z)_{sup}$; 2(*e*) $(x, 1/4, z)_{sup}$; 2(*e*) $(x, 3/4, z)_{sup}$.The O(1) atom (2(*a*)) position, 0, 0, 0) was split in 2(*e*) (≈ 0, 1/4, ≈ 0) and 2(*b*) (0, 1/2, 0) positions.

The Pb(1) atom occupies a 4(*f*) site with the refined occupancy 0.466(5). Pb(2) occupies a 2(*e*) position nearly fully occupied, occ. = 0.892(5). The refined occupancies lead to the same stoichiometry $Pb_{0.30}V_2O_5$. The atomic coordinates were refined and anisotropic thermal parameters were considered for lead and vanadium atoms. The oxygen isotropic displacement parameters were set to their refined values in the subcell otherwise leading to negative values for some of the oxygen atoms. In the last cycles of refinement, secondary extinction was refined yielding the final $R = 0.047$, $R_w = 0.055$. A subsequent Fourier difference calculation did not show evidence of significant residual electronic density. This model takes into account the different DP interatomic vectors. The absence of any observed vectors linking Pb(1) to Pb(2) is justified by the statistical disorder of the former. The Pb(1)–Pb(1) vectors produce the strong maximum and minimum at (0, 1/2, 0.22) and at (0, 1/2, 0), respectively. These should be reduced by the (0, 1/2, 0) Pb(2)–Pb(2) possibility but still appear predominant.

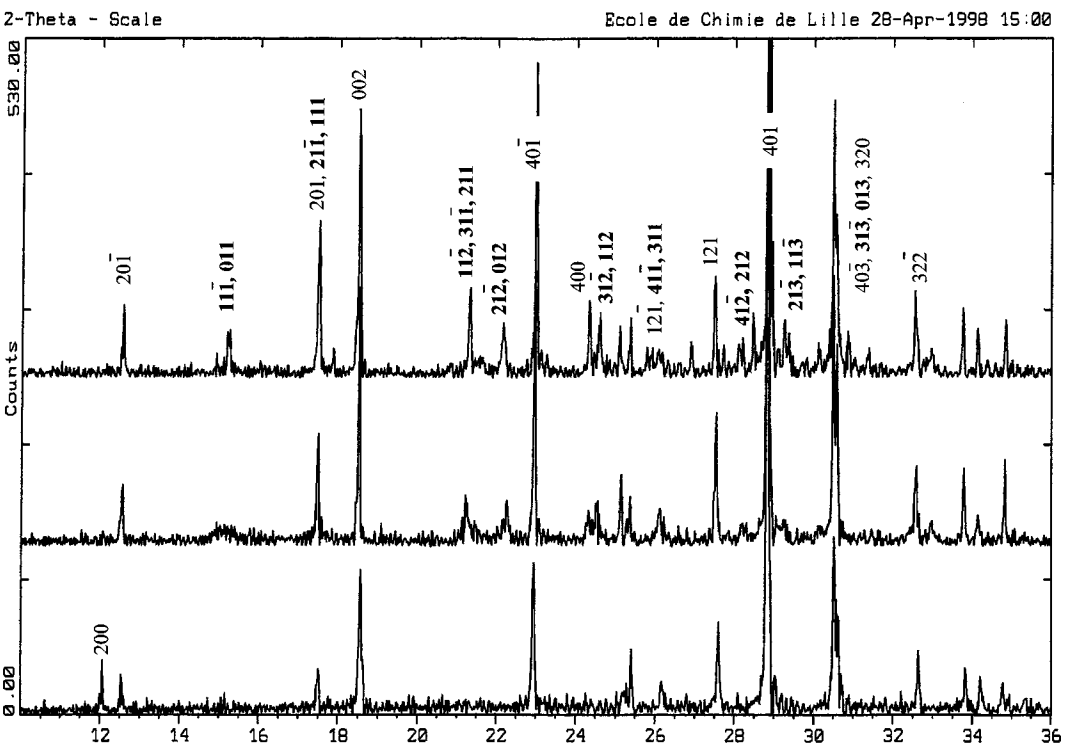

FIG. 3. X-ray powder patterns of β-$Pb_xV_2O_5$ for $x = 0.25$, 0.30, and 0.33. Peaks involving the *b*-doubling are indexed in bold.

Superstructure on Powder Samples

Figure 3 shows the X-ray diffraction powder patterns of $Pb_xV_2O_5$ for $x = 0.25$, 0.30, and 0.33. The lattice parameters refined using a least-square minimization are presented in Table 5. The a parameter and the β-angle slightly decrease vs x while b, c parameters increase leading to the expected raising of the cell volume with higher lead content. Therefore the $x = 0.30$ and 0.33 cell parameters were refined taking account of the number of superstructure lines growing up on the pattern to confirm their assignment. They appear in Fig. 3 as broader peaks (indexed in bold) for $Pb_{0.30}V_2O_5$, indicative of diffuse scattering and get thinner for $Pb_{0.33}V_2O_5$. It is noticeable that their relative intensities match satisfactorily with the powder pattern intensities simulated using the LAZY-PULVERIX program (25) and the $Pb_{0.30}V_2O_5$ crystallographic study data. Note that these calculations predict the existence of the 200 line for a Pb/V ratio of 0.25/2 while its calculated intensity is close to zero for the two richest lead compositions as observed in Fig. 3.

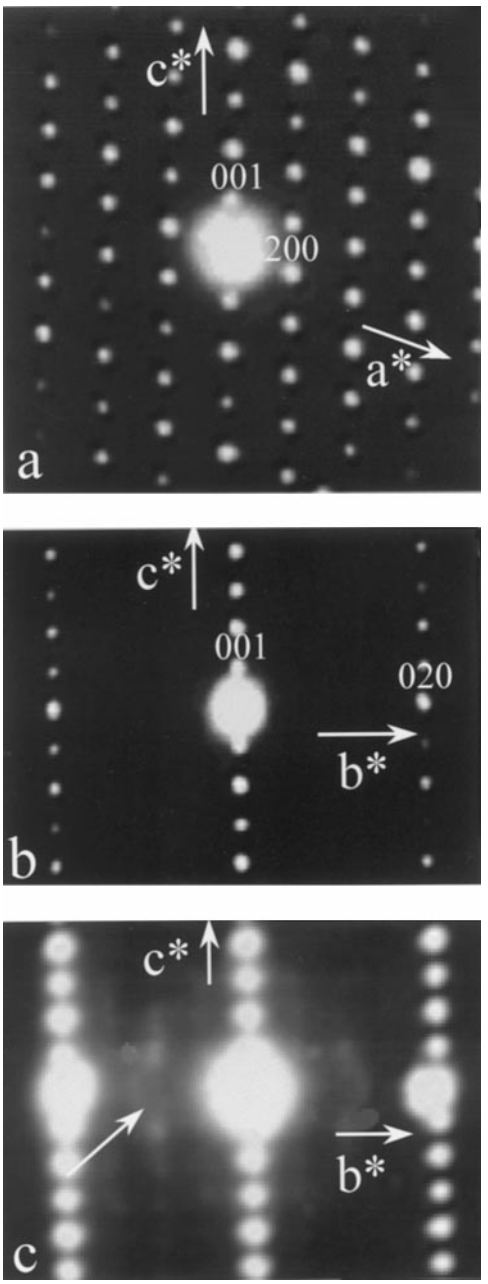

FIG. 4. Electron diffraction pattern of $Pb_{0.25}V_2O_5$ showing the (a) [010], (b) [100], (c) [100] zones of some crystals showing diffuse streaks (arrow).

TABLE 3
Supercell Positional and Isotropic Thermal Parameters

Atom	Site and occupancy	x	y	z	B_{iso} or B_{eq} (Å^2)
Pb(1)	4(f), 0.466(5)	0.5040(1)	0.0032(1)	0.3948(2)	1.97(4)
Pb(2)	2(e), 0.892(5)	0.00453(7)	3/4	0.3944(1)	0.49(1)
V(1)a	4(f), 1	0.8314(3)	0.5012(2)	0.0964(5)	0.64(11)
V(1)b	2(e), 1	0.3391(3)	3/4	0.1008(5)	0.16(9)
V(1)c	2(e), 1	0.3381(3)	1/4	0.0984(5)	0.18(9)
V(2)a	4(f), 1	0.6115(2)	0.4992(2)	0.1112(3)	0.29(5)
V(2)b	2(e), 1	0.1213(3)	3/4	0.1155(4)	0.68(7)
V(2)c	2(e), 1	0.1259(2)	1/4	0.1260(4)	0.45(6)
V(3)a	4(f), 1	0.7800(3)	0.5017(2)	0.4036(4)	0.33(7)
V(3)b	2(e), 1	0.2874(3)	3/4	0.4112(5)	0.44(8)
V(3)c	2(e), 1	0.2906(3)	1/4	0.4144(4)	0.33(7)
O(1)a	2(e), 1	−0.0002(8)	1/4	−0.005(1)	0.97(0)
O(1)b	2(b), 1	1/2	0	0	—
O(2)a	4(f), 1	0.315(1)	0.001(1)	0.054(2)	0.68(0)
O(2)b	2(e), 1	0807(1)	3/4	0.046(2)	—
O(2)c	2(e), 1	0815(1)	1/4	0.045(2)	—
O(3)a	4(f), 1	0.130(1)	0.003(1)	0.075(2)	0.52(0)
O(3)b	2(e), 1	0.637(1)	3/4	0.080(2)	—
O(3)c	2(e), 1	0.637(1)	1/4	0.079(2)	—
O(4)a	4(f), 1	0.939(1)	−0.010(1)	0.217(2)	1.10(0)
O(4)b	2(e), 1	0.432(2)	3/4	0.215(2)	—
O(4)c	2(e), 1	0.430(2)	1/4	0.215(2)	—
O(5)a	4(f), 1	0.760(1)	0.003(1)	0.222(2)	0.58(0)
O(5)b	2(e), 1	0.267(1)	3/4	0.221(2)	—
O(5)c	2(e), 1	0.264(1)	1/4	0.222(2)	—
O(6)a	4(f), 1	0.614(1)	0.003(1)	0.278(2)	1.08(0)
O(6)b	2(e), 1	0.108(1)	3/4	0.269(2)	—
O(6)c	2(e), 1	0.101(1)	1/4	0.265(2)	—
O(7)a	4(f), 1	0.251(1)	0.000(1)	0.423(2)	0.83(0)
O(7)b	2(e), 1	0.756(1)	3/4	0.421(2)	—
O(7)c	2(e), 1	0.766(1)	1/4	0.431(2)	—
O(8)a	4(f), 1	0.892(1)	0.014(1)	0.468(2)	1.27(0)
O(8)b	2(e), 1	0.395(1)	3/4	0.471(2)	—
O(8)c	2(e), 1	0.397(1)	1/4	0.472(2)	—

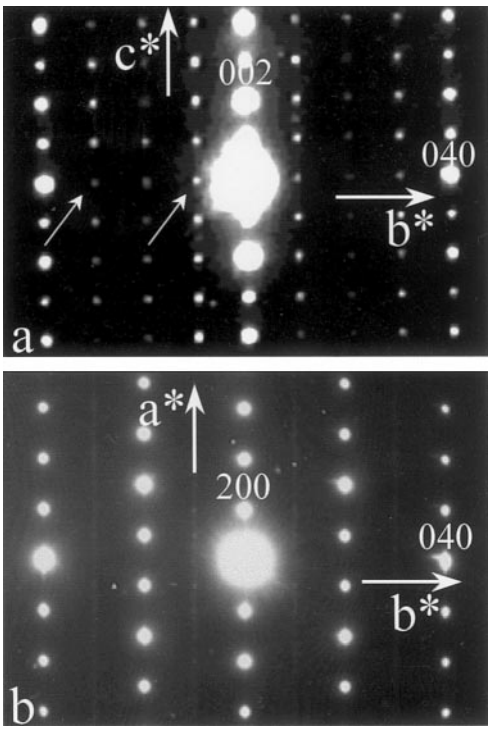

FIG. 5. Electron diffraction pattern of $Pb_{0.30}V_2O_5$ showing the (a) [100] zone; weak spots are superimposed to basic spots involving the *b*-doubling. (b) [001] zone axis; it reveals a weak streaking parallel to *a**, running halfway between the rows of basic reflections.

The ED study is in perfect agreement with the X-ray results. No superstructure spots are evidenced in the $Pb_{0.25}V_2O_5$ sample. The [010] and [100] ED patterns (Figs 4a and 4b) confirm the usual cell parameters found for the vanadium bronze $Pb_xV_2O_5$ and fulfill the C centering conditions. One must note, however, in the [100] EDP of some crystals (Fig. 4c), the presence of diffuse streaks (arrow).

In accordance with the X-ray results, superstructure spots appear on the ED patterns of the higher lead-containing samples. The ED study particularly concerned the $Pb_{0.30}V_2O_5$ compound. Its [100] (Fig. 5a) as well as its [001] (Fig. 5b) ED patterns both show a superstructure whereas no superstructure was evidenced on the [010] ED pattern. In the [100] zone, the most intense spots are basic spots generated by the C centered bronze sublattice. Superimposed on these basic spots, weaker spots were observed leading to a doubling of the *b* parameter. However, the weak $0k0$, $k = 2n + 1$ spots (arrows) are due to double diffraction effects since they disappear after a few degrees rotation around *b**. Thus, reflection conditions are in accordance with the $P2_1/m$ S.G. used in the X-ray refinement. Note the existence of some [100] ED pattern without superstructure spots. This variation in the ED patterns can be attributed to some Pb inhomogeneity in the preparations, a small decrease of the Pb content resulting in no detectable superstructure formation.

For $Pb_{0.30}V_2O_5$, the [001] ED pattern reveals a weak streaking parallel to *a**, running halfway between the rows of basic reflections (Fig. 5b). This diffuse intensity is compatible with a cell doubling along the *b* axis, but such that the correlation along *a* (between two successive tunnels), is largely lost. The weak intensity of these streaks reveals the high degree of disorder existing along this direction. Unfortunately, attempts to get high resolution images failed because of the systematic and instantaneous amorphization of the sample under focused beam.

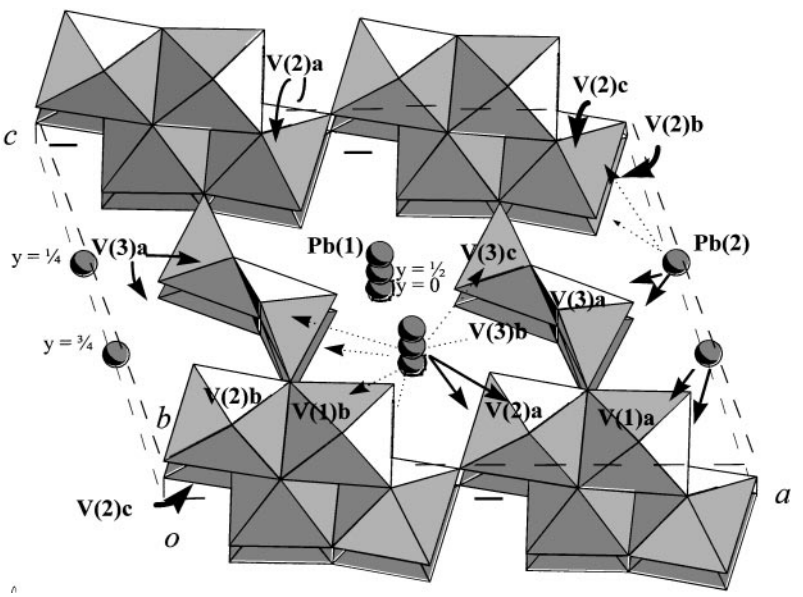

FIG. 6. $Pb_{0.30}V_2O_5$ crystal structure representation in the (*ac*) plane. The arrows starting from Pb atoms indicate weak (dotted lines) and strong (bold lines) interactions.

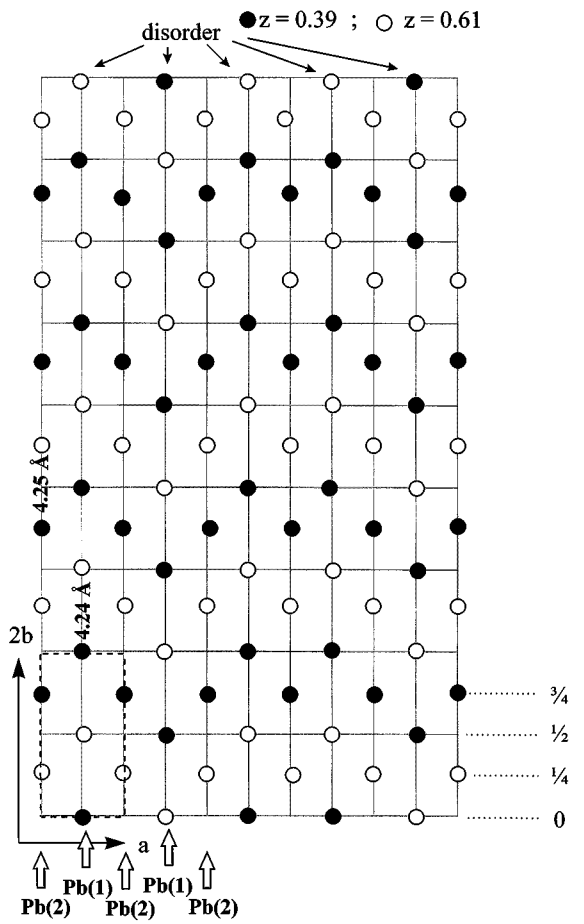

FIG. 7. Cationic sequence along the 2*b* axis. Pb(1) periods are shifted from each other.

DISCUSSION

Structure Description

The structure of β-bronze was first determined by Wadsley from a single crystal of $Na_{0.33}V_2O_5$. Within the subcell V–O framework, the vanadium ions occupy two distinguishable octahedral sites in which the V–O distances vary from 1.61 to 2.30 Å and a triangular bipyramidal site with V–O distances, goes from 1.60 to 1.99 Å (a sixth atom is located at 2.60 Å). By edge sharing, the oxygen polyhedra form double octahedral-site chains and single bipyramidal-site chains. The corner sharing of the different chains produces true tunnels with Pb^{2+} hosts (Fig. 6). Because of the split of atomic positions to several independent atoms, the V–O distances become much more contrasted under the supercell considerations, as discussed below (Table 3).

Pb^{2+} Ordering

As already pointed out by Darriet *et al.*, because of its large ionic radius Pb^{2+} cannot occupy two next 4(*i*) positions of the average structure, 0.22 *c* distant (15). This would lead to a too short Pb–Pb distance of 2.1 Å considering the repulsive interaction in the tunnels. One possible way of maximizing occupancy is to have an ordered Pb^{2+} zigzag sequence along *b* with only one kind of intertunnel Pb–Pb vector of coordinates 0, 1/2, $\pm$ 0.22. This ordering pattern relates Pb(2) atoms leading to one kind of Pb(2)–Pb(2) distance, 4.251(1) Å long. In the refined arrangement, an

TABLE 4
Main Interatomic Distances (Å) for $Pb_{0.30}V_2O_5$ in the Sub- (bold) and Supercell

Pb–O(4)^{v}	2.539(3)	Pb_a–O(4)$_b$	2.573(13)	Pb_b–O(4)$_b$	2.472(13)		
Pb–O(4)^{v}	2.539(3)	Pb_a–O(4)$_c$	2.546(13)	Pb_b–O(4)$_c$	2.472(13)		
Pb–O(6)	2.346(6)	Pb_a–O(6)$_a$	2.372(20)	Pb_b–O(6)$_a$	2.349(20)		
Pb–O(8)^{vi}	2.497(3)	Pb_a–O(8)$_b$	2.474(10)	Pb_b–O(8)$_b$	2.448(11)		
Pb–O(8)^{vi}	2.497(3)	Pb_a–O(8)$_c$	2.491(10)	Pb_b–O(8)$_c$	2.448(11)		
V(1)–O(2)^{ii}	2.304(4)	$V(1)_a$–O(2)$_a$	2.275(14)	$V(1)_b$–O(2)$_c$	2.355(14)	$V(1)_c$–O(2)$_b$	2.239(14)
V(1)–O(2)^{v}	1.880(1)	$V(1)_a$–O(2)$_b$	1.888(5)	$V(1)_b$–O(2)$_a$	1.896(8)	$V(1)_c$–O(2)$_a$	1.875(5)
V(1)–O(2)^{v}	1.880(1)	$V(1)_a$–O(2)$_c$	1.897(5)	$V(1)_b$–O(2)$_a$	1.896(8)	$V(1)_c$–O(2)$_a$	1.875(8)
V(1)–O(3)^{v}	1.989(5)	$V(1)_a$–O(3)$_a$	2.013(22)	$V(1)_b$–O(3)$_c$	1.973(22)	$V(1)_c$–O(3)$_b$	1.967(22)
V(1)–O(4)	1.610(4)	$V(1)_a$–O(4)$_a$	1.711(14)	$V(1)_b$–O(4)$_b$	1.519(24)	$V(1)_c$–O(4)$_c$	1.519(23)
V(1)–O(5)	1.937(5)	$V(1)_a$–O(5)$_a$	1.941(22)	$V(1)_b$–O(5)$_b$	1.903(22)	$V(1)_c$–O(5)$_c$	1.957(22)
V(2)–O(1)	1.806(1)	$V(2)_a$–O(1)$_b$	1.721(3)	$V(2)_b$–O(1)$_a$	1.839(11)	$V(2)_c$–O(1)$_a$	1.965(11)
V(2)–O(2)^{ii}	2.299(5)	$V(2)_a$–O(2)$_a$	2.312(21)	$V(2)_b$–O(2)$_c$	2.161(22)	$V(2)_c$–O(2)$_b$	2.303(22)
V(2)–O(3)^{v}	1.895(1)	$V(2)_a$–O(3)$_b$	1.918(6)	$V(2)_b$–O(3)$_a$	1.903(9)	$V(2)_c$–O(3)$_a$	1.880(9)
V(2)–O(3)^{v}	1.895(1)	$V(2)_a$–O(3)$_c$	1.909(7)	$V(2)_b$–O(3)$_a$	1.903(9)	$V(2)_c$–O(3)$_a$	1.880(9)
V(2)–O(5)	2.154(4)	$V(2)_a$–O(5)$_a$	2.200(14)	$V(2)_b$–O(5)$_b$	2.153(15)	$V(2)_c$–O(5)$_c$	2.035(14)
V(2)–O(6)	1.632(5)	$V(2)_a$–O(6)$_a$	1.676(21)	$V(2)_b$–O(6)$_b$	1.633(22)	$V(2)_c$–O(6)$_c$	1.577(22)
V(3)–O(5)	1.802(4)	$V(3)_a$–O(5)$_a$	1.761(21)	$V(3)_b$–O(5)$_b$	1.845(21)	$V(3)_c$–O(5)$_c$	1.853(20)
V(3)–O(7)^{ii}	1.994(6)	$V(3)_a$–O(7)$_a$	1.967(22)	$V(3)_b$–O(7)$_a$	1.922(9)	$V(3)_c$–O(7)$_a$	1.933(9)
V(3)–O(7)^{v}	1.892(1)	$V(3)_a$–O(7)$_b$	1.867(5)	$V(3)_b$–O(7)$_a$	1.922(9)	$V(3)_c$–O(7)$_a$	1.933(9)
V(3)–O(7)^{v}	1.892(1)	$V(3)_a$–O(7)$_c$	1.878(5)	$V(3)_b$–O(7)$_c$	2.026(22)	$V(3)_c$–O(7)$_b$	2.022(22)
V(3)–O(8)	1.607(4)	$V(3)_a$–O(8)$_a$	1.642(15)	$V(3)_b$–O(8)$_b$	1.573(15)	$V(3)_c$–O(8)$_c$	1.555(15)

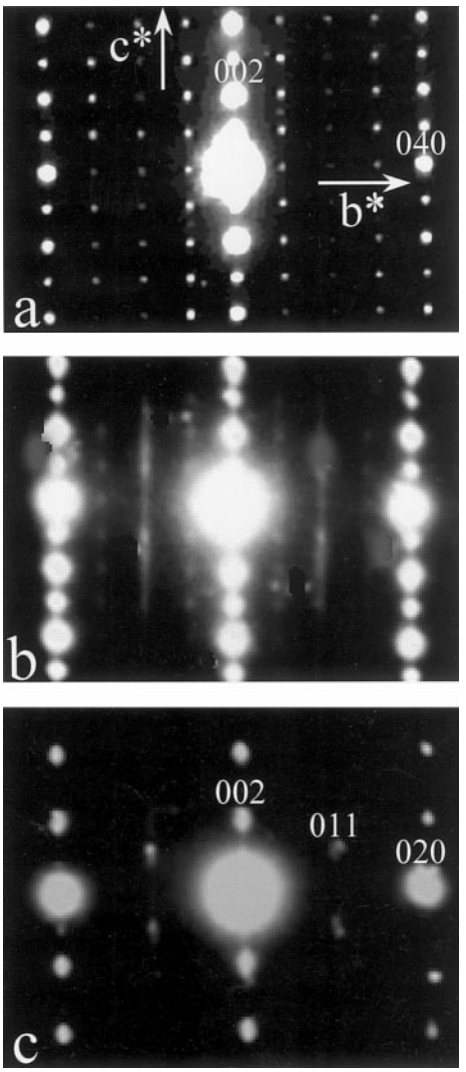

FIG. 8. [100] ED pattern for $Pb_{0.30}V_2O_5$ at (a) room temperature, indexed with the double b axis; (b) 525°C, note weakening of the superlattice spots; (c) during cooling, indexation is performed in the subcell.

additional Pb–Pb vector $1/2b$ could sometimes intervene. It could be assigned to an intratunnel antiphase boundary in the zigzag scheme that has already been described. Therefore, like the $0.22c$ vector, $b/2$, 3.65 Å long, may be too short to be a viable nonbounded Pb–Pb distance. Furthermore, the 0, 1/2, 0 vector appeared as a minimum on the DP map refuting intratunnel antiphase boundary existence. In other words, the crystal structure determination results denote an ordered cationic sequence running along the b axis over half of the infinite tunnels whereas the remaining part seems to be disordered in average over the sample. The Pb(1) statistic distribution within the channels is a formal model deduced from the X-ray study but is not completely satisfying. As a matter of fact, the Pb(1) and Pb(2) occupancy being similar, 0.466/2 and 0.892/4, respectively, the zigzag sequence observed in Pb(2) tunnels is likely viewable for Pb(1) atoms. Thus, the two independent tunnels would accommodate the same Pb^{2+} sequence but a random $b_{subcell}$ shift would operate between Pb(2) tunnels leading to an average X-ray detected statistic distribution for these atoms (Fig. 7).

V–O Framework Distortion

All of the vanadium oxygen polyhedra exhibit among their coordination distances a short V–O bond that is oriented toward the free oxygen apex located at the internal boundary limit of the tunnels. Such distances are assigned to V=O vanadyl double bond often observed in the mixed vanadium compounds. As observed in Table 4, the split of equivalent vanadium and oxygen atoms in three independent positions of the supercell considerably modifies these significant V–O distances. As a matter of fact, the sublattice short V(1)–O(4), V(2)–O(6), and V(3)–O(8) of 1.610(4) Å, 1.632(5) Å, and 1.607(4) Å, respectively, are split in supercell into triplets of three various distances: 1.711(14)/1.519(24)/1.519(23) Å, 1.676(21)/1.633(22)/1.577(22) Å, and 1.642(15)/1.573(15)/1.555(15) Å, respectively. In Fig. 6, the different effects of disordered Pb(1) and ordered Pb(2) can be seen. Pb(1) induces a strong repulsive effect on $V(2)_a$ while the shortest V=O (for the $V(1)_b$, $V(1)_c$, $V(3)_b$, and $V(3)_c$ atoms) indicates only slight interaction. The opposite phenomenon occurs in the neighboring tunnel with strong $Pb(2) \rightarrow V(1)_a$ and $Pb(2) \rightarrow V(3)_a$, repulsions but weak $Pb(2) \rightarrow V(2)_b/V(2)_c$ interactions (Table 4).

Thermal Behavior

We performed *in situ* heating of the $Pb_{0.3}V_2O_5$ sample using the heating stage of the electron microscope. The temperatures are to be considered approximate because of the large experimental error in their measurement. Figure 8 represents the evolution of the [100] ED pattern versus temperature. A transition (Fig. 8a → Fig. 8b) occurs at around 525°C and is characterized by a progressive disappearance of the weak spots responsible for the b-axis doubling. An extra irreversible phenomenon (Fig. 8c) occurs on cooling at 445–470°C and is evidenced by the

TABLE 5
Unit Cell Parameters vs x in β-$Pb_xV_2O_5$

x	a (Å)	b (Å)	c (Å)	β(°)	V(Å$_3$)
0.25	15.501(4)	7.269(2)/2	10.105(3)	109.29(1)	1074.6/2
0.30	15.478(10)	7.288(5)	10.123(6)	109.27(3)	1077.9
0.33	15.473(5)	7.301(3)	10.128(4)	109.23(2)	1080.3

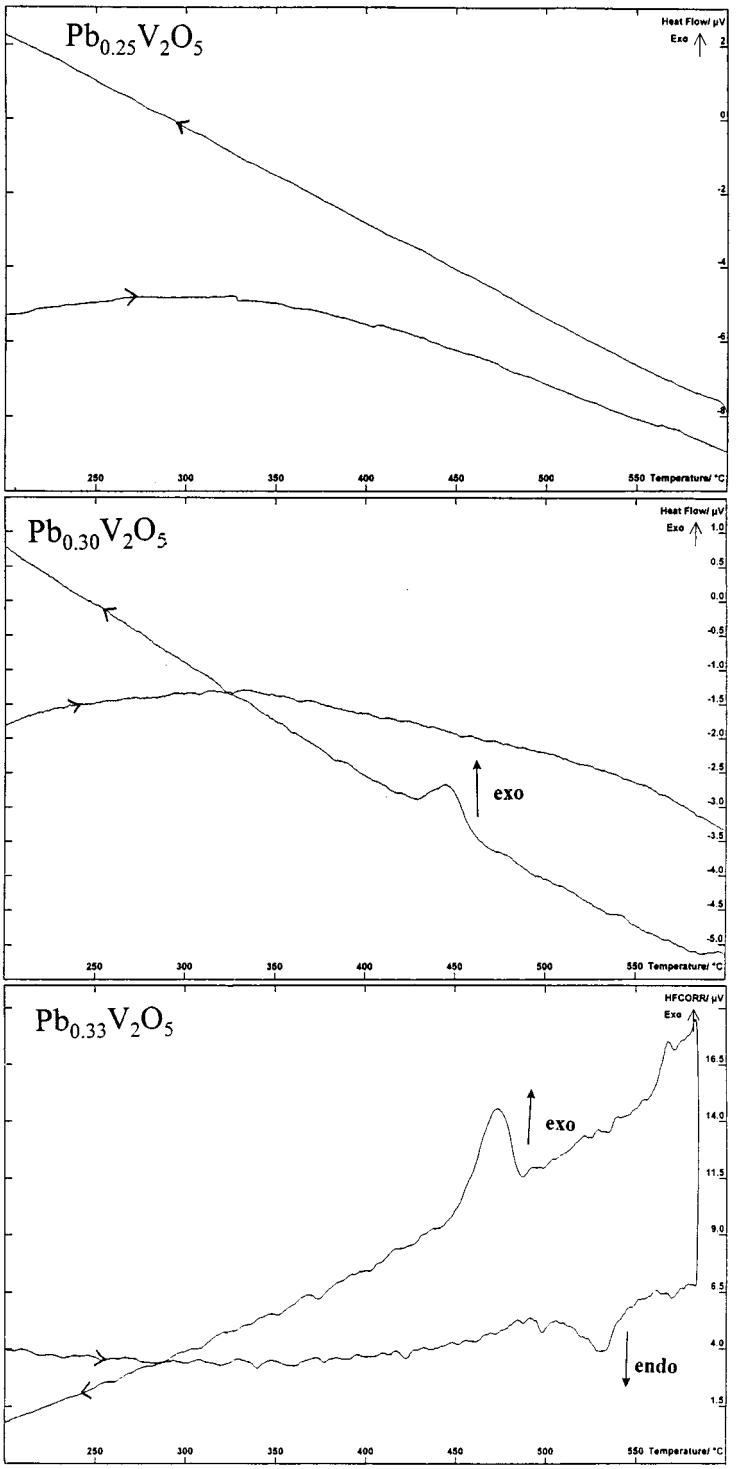

FIG. 9. DTA plots for the three noted compositions.

disappearance of the fundamental $0kl$, $k + l = 2n + 1$ spots whereas the C-centered condition is no more respected (011 spot indexation). The behavior is not yet understood but seems to involve an *n*-glide perpendicular to the *a*-axis. In order to confirm such evolution DTA measurements were performed.

Figure 9 presents the DTA plots obtained for the three samples on both heating and subsequent cooling at a rate of

5°C/min. The experiment was carried out from room temperature to 575°C to avoid melting of the sample. A strong nitrogen flow was necessary to protect our samples from oxidation. A sample condition was simultaneously monitored by TGA. As expected, no thermal phenomenon was detected for $Pb_{0.25}V_2O_5$. On the other hand, $Pb_{0.33}V_2O_5$ undergoes an endothermic event on heating at around 530°C that we undoubtly assign to the cationic order–disorder transition described above. Astonishingly, the $Pb_{0.30}V_2O_5$ thermal analysis plot did not show evidence of the endothermal behavior, despite the disappearance of superlattice reflections on heating observed for a few crystallites of this composition. This is explained if the relatively weak and diffuse features of the supercell lines on the $x = 0.30$ X-ray diffraction pattern are associated with a strong dilution of the DT peak. Moreover, perfect homogeneity of the lead content within the sample cannot be guaranteed and the presented ED patterns for this sample could have been obtained from crystallites with $x > 0.30$. Then, for both $x = 0.33$ and $x = 0.30$ a very strong exothermal peak occurs on cooling around 470 and 445°C, respectively. It is probably related to the development of *n*-glide absences on the [100] zone axis ED. Considering the three samples, this behavior seems superstructure-independent since it ensues from a high-temperature disordered cationic state. The lack of DTA-signal on cooling for $Pb_{0.25}V_2O_5$ is consistent with the Pb content in this material being too low for ordering to occur. An X-ray diffraction powder pattern of the DTA residue was collected, but was of poor quality. Indeed, peaks were very broad and low in height and superimposed on a large background. However, one can deduce a textural change of the sample and at least observe the disappearance of the superstructure lines for $x = 0.30$ and 0.33 (Table 5).

a-Axis Doubling

As already mentioned in the Experimental section, for one of the number of tested crystals, the *h*1*l* layer Weissenberg photograph showed evidence of 2*a* spots tied on diffuse streaks parallel to *a** (Fig. 10). Such features were not observed on fundamental *h*0*l* and *h*2*l* layers indicating an *a*-doubling subcondition of the *b*-doubling. In the discussion below all *hkl* Miller indices are indexed on the large 2*a*, 2*b*, *c* unit cell. In the diffraction pattern of Fig. 10, *h*1*l* are absent for $h + k = 4n$ while the existing reflections often appear as brighter zones along the diffuse streaks. The electron diffraction patterns taken on some crystallites of the $Pb_{0.33}V_2O_5$ nominal samples (Fig. 11) are in good agreement with our X-ray study where the *hk*0 layer [001] zone axis for this compound exhibits the absences for $h + k = 4n$. Considering these extinctions a general rules can be established involving the unusual $(h - k) = 4n + 2$ systematic extinction for supercell *hkl* planes, *h* and *k* odd. This is related to the existence of a cationic-only $1/4\,(a - b)$ translation. The validity of this hypothesis was tested in the 2*a*, 2*b*, *c* unit cell by simulating every possible Pb^{2+} arrangement with a theoretical intensity lines calculation. Our LAZY-PULVERIX results were in good agreement with the observed photograph in term of existing and absent peaks solely for the model presented on Fig. 12. Thus, in fully ordered β-$Pb_xV_2O_5$, the lead atoms line up parallel to the [1 $\bar{1}$ 0] direction at alternately $z \approx 0.31$ and $z \approx 0.69$. Two subsequent Pb^{2+} of the so-called lines belong to two distinct tunnels leading to strong intratunnel electrostatic interactions. Intertunnel ordering is relatively rarely observed in oxides because of the strong shielding effects of tunnels walls. It is observed in hollandite-type compounds that often display superstructure or diffuse scattering in diffraction patterns. It is in most cases

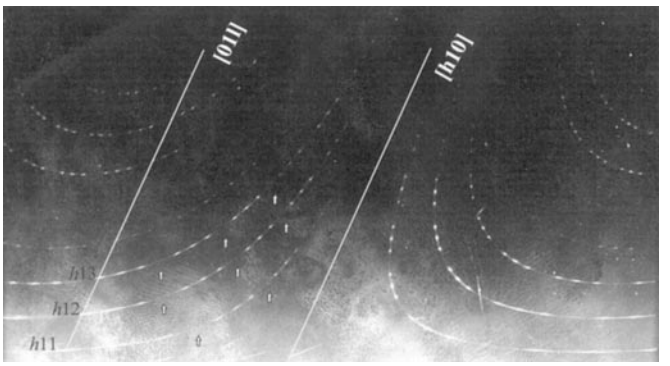

FIG. 10. Weissenberg photograph of the (*h*1*l*) layer. The reciprocal lattice rows are indexed in the (2*a*, 2*b*, *c*) fourfold unit cell. Some absent $(h - k) = 4n + 2$ reflections are marked by arrows.

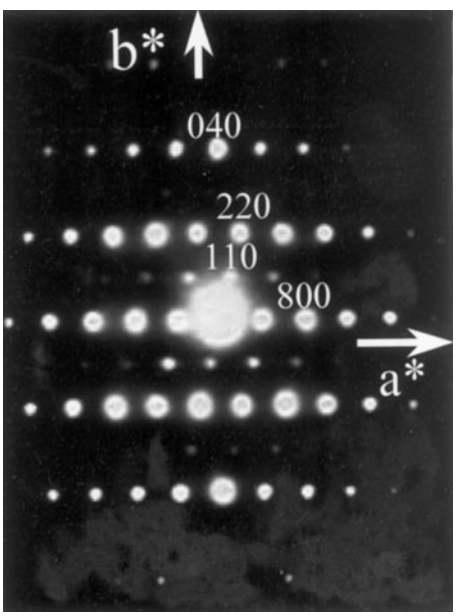

FIG. 11. [001] zone ED pattern for $Pb_{0.33}V_2O_5$. The pattern exhibits the *a* and *b* parameters doubling and is indexed in the fourfold unit cell.

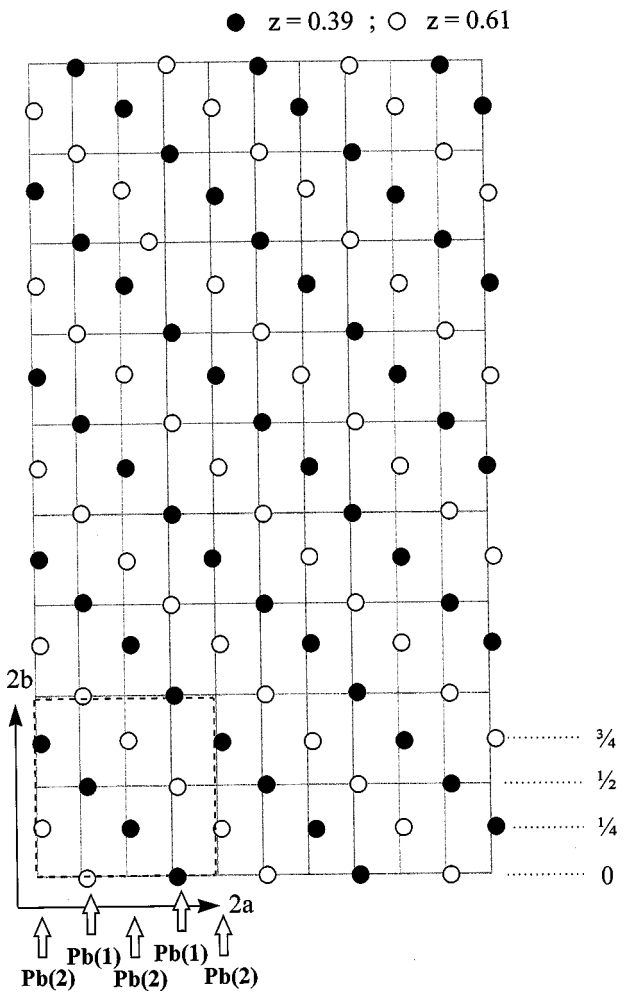

FIG. 12. Predicted ideal bidimensionally ordered bronze.

due to a one-dimensional ordering in which cations are intratunnel ordered with no correlation between tunnels (26). An extreme case of the superstructure is also known where both intra- and intertunnel orderings cohabitate (27). In Pb-vanadium bronzes, such ordering is likely to produce strong lattice distorsion. Effectively the vacancies and cation periodicity induces a commensurate wave of electronic density adopted by the V–O framework. The complex arrangement of the Pb^{2+} in the bronzes framework is mainly due to the high polarizability of Pb^{2+}. As a matter of fact, the presence of its $6s^2$ stereoactive lone pair is in favor of commensurate or incommensurate ordering in mineral lattice.

ACKNOWLEDGMENT

The authors sincerely thank Professor Van Tendeloo (EMAT, University of Antwerp, Belgium) for interesting and useful discussions.

REFERENCES

1. J. H. Perlstein and M. J. Sienko, *J. Chem. Phys.* **48,** 174 (1968).
2. J. B. Goodenough, *J. Solid State Chem.* **1,** 349 (1970).
3. B. K. Chakraverty, M. J. Sienko, and J. Bonnerot, *Phys. Rev. B* **17,** 3781 (1978).
4. P. Hagenmuller, *in* "Non Stoichiometric Compounds, Tungsten Bronzes, Vanadium Bronzes and Related Compounds" (D. J. Bevan and P. Hagenmuller, Eds.), Vol. 1, p. 569. Pergamon Press, Oxford, 1973.
5. A. Hardy, J. Galy, A. Casalot, and M. Pouchard, *Bull. Soc. Chim. Fr.* 1056 (1965).
6. P. Hagenmuller, J. Galy, M. Pouchard, and A. Casalot, *Mat. Res. Bull.* **1,** 45 (1966).
7. J. Galy, M. Pouchard, A. Casalot, and P. Hagenmuller, *Bull. Soc. Fr. Min. Crist.* **XC,** 544 (1967).
8. J. Galy, J. Darriet, A. Casalot, and J. B. Goodenough, *J. Solid State Chem.* **1,** 339 (1970).
9. J. Galy, J. Darriet, and P. Hagenmuller, *Rev. Chim. Miner.* **8,** 509 (1971).
10. K. Wiesener, W. Schneider, D. Ilic, E. Steger, K. H. Hallmeir, and E. Brackmann, *J. Power Sources* **20,** 157 (1978).
11. J. Labat, M. Broussely, and J. Bodet, *Proc. ASEE PARIS*, 1989.
12. P. Millet, C. Satto, P. Sciau, and J. Galy, *J. Solid State Chem.* **136,** 56 (1998).
13. R. Enjalbert and J. Galy, *Acta Cryst. C* **42,** 1467 (1986).
14. P. Rozier, J. M. Savariault, J. Galy, C. Marichal, J. Hirschinger, and P. Granger, *Eur. J. Solid State Inorg. Chem.* **33,** 1 (1995).
15. J. Darriet, R. Von Der Mühll, and J. Galy, *Bull. Soc. Fr. Mineral. Cristallogr.* **92,** 17 (1969).
16. A. D. Wadsley, *Acta Cryst.* **23,** 558 (1967).
17. K. Kato, K. Kosuda, T. Koga, and H. Nagasawa, *Acta Cryst. C* **46,** 1587 (1990).
18. J. Kakinoki and Y. Komura, *Acta Cryst.* **19,** 695 (1955).
19. O. Mentre, A. C. Dhaussy, F. Abraham, and H. Steinfink, *J. Solid State Chem.* **140,** 417 (1998).
20. J. De Meulenaer and H. Tompa, *Acta Cryst.* **19,** 1014 (1965).
21. "International Tables for X-Ray Crystallography," Vol. IV. Kynoch Press, Birmingham, 1974.
22. D. T. Cromer and D. Liberman, *J. Chem. Phys.* **531,** 1891 (1970).
23. C. T. Prewitt, "SFLS-5, Report ORNL-TM 305," Oak Ridge National Laboratory, Oak Ridge, TN, 1966.
24. A. J. Frueh, *Acta Cryst.* **6,** 454 (1953).
25. K. Yvon, W. Jeitscho, and E. Parthe, *J. Appl. Cryst.* **10,** 73 (1977).
26. A. J. Frueh, *Acta Cryst.* **6,** 454 (1953).
27. L. A. Bursill and G. Grzinic, *Acta Cryst. B* **36,** 2902 (1980).
28. J. Vicat, E. Fanchon, P. Strobel, and D. Tran Qui, *Acta Cryst. B* **42,** 162 (1986).